

## Kinetic-Energy Distribution of Negative Ions Formed by Dissociative Attachment and the Measurement of the Electron Affinity of Oxygen\*

P. J. CHANTRY AND G. J. SCHULZ†

*Westinghouse Research Laboratories, Pittsburgh, Pennsylvania*

(Received 14 November 1966)

The kinetic-energy distribution of ions produced by a dissociative ionization process is derived, taking into account the effect of thermal motion of the target molecule. In the case of dissociative attachment of monoenergetic electrons to a diatomic molecule, the width at half-maximum of the negative-ion energy distribution is given by  $(11\beta kTE_0)^{1/2}$ , where  $\beta$  is the ratio of the mass of the ion to that of the parent molecule,  $T$  is the target-gas temperature, and  $E_0$  is the most probable ion energy. Using a crossed-field velocity filter,  $O^-$  ion energy distributions arising from the attachment of essentially monoenergetic electrons to  $O_2$  are studied as a function of electron energy at two gas temperatures. The measured widths of the distributions are consistent with the above relationship. Measurements of  $E_0$  as a function of the electron energy allow a determination of the electron affinity  $A$  of atomic oxygen. The result,  $A = 1.5 \pm 0.1$  eV, is in excellent agreement with photodetachment-threshold determinations.

**E**LECTRON-BEAM experiments have been used repeatedly for a study of negative-ion formation resulting from dissociative attachment. In particular, measurements of the magnitude of the cross section and the kinetic energy of the fragment ions are of interest. The electron energy dependence of the cross section is of value in determining the potential-energy curve<sup>1</sup> of the molecular negative-ion compound state along which dissociation occurs. The position of this curve at infinite internuclear separation can be determined from the electron energy dependence of the fragment-ion kinetic energy. If the dissociation energy of the neutral molecule is known, this provides a determination of the electron affinity involved. The present paper is concerned primarily with this second aspect of the problem.

In some cases the electron affinity has been determined by other methods, such as photodetachment, and from such comparisons it has become apparent that a serious discrepancy exists between the electron affinity of atomic oxygen as determined from photodetachment

experiments and the value from electron-beam experiments. An attempt to resolve this discrepancy by improving the procedure used in electron-beam experiments (more reliable electron and ion energy scale calibration and improved ion collection efficiency) has not lessened the discrepancy.<sup>2</sup> Whereas the value of the electron affinity of atomic oxygen obtained from photodetachment experiments<sup>3</sup> was 1.465 eV, the values from previous electron-beam experiments centered about 2.0 eV.

We have recently pointed out<sup>4</sup> that this discrepancy in the values of the electron affinity resulted from an incorrect interpretation of ion retarding curves which are often used to determine the ion kinetic energy in electron-beam experiments. In this paper we present a more detailed treatment of the theory involved in the interpretation of such experiments. The experimental work reported in this paper was undertaken in order to demonstrate certain features of the theory, and also to develop techniques for the proper determination of electron affinities from electron-beam experiments. For this purpose we study the  $O_2$  molecule, because it serves as a good example of our considerations and because considerable work has been done on it in the past.

In Sec. I of this paper we discuss the theory appropriate to fragment-ion kinetic-energy considerations in dissociative attachment. In Sec. II the apparatus and experimental techniques employed to measure such kinetic-energy distributions are described. The results of these studies are presented in Sec. III. The theoretical derivation of the fragment-ion kinetic-energy distribution is presented in an Appendix.

\* This research was supported in part by the Advanced Research Projects Agency through the U. S. Office of Naval Research.

† Present address: Yale University, New Haven, Connecticut.

<sup>1</sup> In the study of dissociative ionization processes the position of the relevant potential-energy curve in the Franck-Condon region is often determined by the reflection method. This consists of drawing the curve so that the distribution in kinetic energy of the fragments is given by the reflection of the square of the ground-state vibrational wave function in the potential-energy curve onto the energy axis. [See for example H. D. Hagstrum and J. T. Tate, *Phys. Rev.* **59**, 354 (1941).] Because of the resonant nature of dissociative attachment this procedure may be carried through without a knowledge of the kinetic energy of the fragments, requiring instead that the reflection method reproduce the electron energy dependence of the cross section on the energy axis. The potential-energy curve so derived is however likely to be seriously in error, since the method implicitly assumes that the survival probability against autodetachment of the compound state to complete dissociation is independent of initial internuclear separation, i.e., electron energy. This is unlikely to be the case, and the method gives only a first approximation to the compound-state potential-energy curve. Determination of its true position must also involve a determination of the probability of autodetachment as a function of internuclear separation. For a detailed application of these considerations see T. F. O'Malley, *Phys. Rev.* **155**, 59 (1967).

<sup>2</sup> For a recent review, and references regarding this problem, see G. J. Schulz, *Phys. Rev.* **128**, 178 (1962).

<sup>3</sup> L. M. Branscomb, D. S. Burch, S. J. Smith, and S. Geltman, *Phys. Rev.* **111**, 504 (1958); for a review see L. M. Branscomb, *Atomic and Molecular Processes*, edited by D. R. Bates (Academic Press Inc., New York, 1962), Chap. 4.

<sup>4</sup> P. J. Chantry and G. J. Schulz, *Phys. Rev. Letters* **12**, 449 (1964).

### I. THEORY

Let us consider the reaction in which an electron interacts with a molecule  $XY$  forming the negative ion  $X^-$  and a neutral fragment  $Y$ :



In the center-of-mass system, the excess energy of the reaction  $E_R$  is given by

$$E_R = V_e - (D - A), \quad (2)$$

where  $V_e$  is the kinetic energy available in the center-of-mass system,  $D$  is the dissociation energy of  $XY$ , and  $A$  is the electron affinity of the atom  $X$ . Because of the large ratio of the mass of  $XY$  to that of the electron, the center of mass of the reacting system essentially coincides with the center of mass of  $XY$  and moves relative to the laboratory system with the thermal velocity of  $XY$ . This velocity is in general very much less than the electron velocity, with the result that  $V_e$  is essentially the electron energy measured in the laboratory.

For the purpose of this discussion we shall assume that prior to the reaction the molecule  $XY$  is in its ground state, and that the fragments  $X^-$  and  $Y$  are formed in their ground states. In this case, the total amount of the excess energy  $E_R$ , given by Eq. (2), must appear as kinetic energy of separation of the two fragments, and will be divided between them so as to impart equal and opposite momenta to  $X^-$  and  $Y$  in the center-of-mass system. Thus the ion  $X^-$  will receive kinetic energy  $E_0$  given by

$$E_0 = (1 - \beta)[V_e - (D - A)], \quad (3)$$

where  $\beta = m/M$ ,  $m$  and  $M$  being the masses of  $X^-$  and  $XY$ , respectively. The energy of the ion measured in the laboratory system may be obtained by adding vectorially the initial thermal velocity of  $XY$  to the center-of-mass velocity of  $X^-$ , corresponding to  $E_0$ , and will therefore depend on both the magnitude and orientation of the initial thermal velocity. This effect produces a relatively large spread in the ion energy,<sup>4</sup> measured in the laboratory. Thus, it is clear that, while the thermal motion of the target gas may be neglected when calculating the energy balance of the reaction, it does play a significant role in determining the fraction of the total excess energy  $E_R$  which appears as kinetic energy of a given fragment in the laboratory.

If the thermal motion of  $XY$  is neglected entirely, one concludes that the fragment ions are monoenergetic when monoenergetic electrons are used, their energy being given by Eq. (3). This assumption has, in the past, led to an incorrect interpretation of retarding curve measurements used for determining the negative-ion kinetic energy, giving erroneously high values for the electron affinity involved.

If one assumes that the target molecules have a Maxwellian distribution of velocities corresponding to

a gas temperature  $T$ , one may show that provided  $E_0 \gg kT$ , the fragment of mass  $m$  has an energy distribution in the laboratory system given by

$$\frac{dN}{N} = \left( \frac{1}{4\pi\beta kTE_0} \right)^{1/2} \exp \left[ -\frac{1}{\beta kT} (E^{1/2} - E_0^{1/2})^2 \right] dE. \quad (4)$$

The exact form of the distribution function, applicable without the restriction on  $E_0$ , is derived in the Appendix. In the case of  $O^-$  production from  $O_2$  at room temperature,  $E_0$  always exceeds  $kT$  by at least a factor of 10 and use of Eq. (4) is justified.

Inspection of Eq. (4) shows that the distribution peaks at  $E = E_0$ , and that the half-maximum points occur at  $E_0 + 0.69\beta kT \pm 2(0.69\beta kTE_0)^{1/2}$  corresponding to an energy width at half-maximum  $W_{1/2}$  given by

$$W_{1/2} = (11\beta kTE_0)^{1/2}. \quad (5)$$

Using Eqs. (3) and (5) we may obtain a relation between  $W_{1/2}$  and  $V_e$ :

$$W_{1/2}^2 = 11\beta(1 - \beta)kT[V_e - (D - A)]. \quad (6)$$

The significant width of this distribution has to be taken into account when attempting to interpret retarding curves taken on the fragment ion. In order to do so it is necessary to know the acceptance angle of the retarding system employed, the gas temperature, and the angular distribution of the dissociation products. In attempting to interpret existing experimental data,<sup>4</sup> these factors are usually unknown. In much of the published data the complete retarding curves have in any case not been taken. Rather, the "appearance potential" of the negative ions has been measured as a function of the applied retarding potential. Interpretation of such data requires further assumptions regarding detection sensitivity and the procedure adopted in determining these appearance potentials. The results of any such interpretation are therefore subject to certain necessary assumptions. The number of assumptions could clearly be reduced by repetition of the experiments under known conditions of temperature and acceptance angle. In general, however, the angular distribution of the dissociation products remains unknown<sup>5</sup> and must still be assumed in order to derive the ion energy distribution from the retarding curves.<sup>6</sup>

On the other hand, a direct measurement of the position of the peak of the ion kinetic-energy distribution determines  $E_0$  directly. Thus we conclude that in order to preserve the simplicity of interpretation inherent in the use of Eq. (3), it is necessary to measure the position of the peak of the ion-energy distribution as a function of electron energy.

<sup>5</sup> G. H. Dunn, Phys. Rev. Letters 8, 62 (1962).

<sup>6</sup> In cases where the dissociation energy and electron affinity are known, it is possible in principle to determine the angular distribution of the products from an analysis of the shape of the ion retarding curves observed in an apparatus of known large acceptance angle.

## II. EXPERIMENT

A diagram of the apparatus used in the present studies is shown in Fig. 1. The gas being studied, in this case oxygen, enters the collision chamber through a copper tube of 1.2 cm outside diameter and 0.3 cm inside diameter and of total length 28 cm, of which 8 cm projects outside the vacuum wall of the system. The external part of the copper tube is surrounded by a Dewar vessel in order that, when required, the copper tube may be cooled with liquid nitrogen. Within the vacuum system the copper tube terminates in a small flange to which is bolted a 6-mm-thick plate which forms one wall of the collision chamber and serves also to support the rest of the electrodes shown in the diagram.

The electron beam, whose direction is perpendicular to the diagram, is produced by a thoria coated iridium filament and collimated by an electrode system which permits the use of the retarding potential-difference (R. P. D.) technique<sup>7</sup> for reducing the effective energy distribution of the electron beam. A rather large electromagnet aligns the electron beam and bathes the region indicated by the crosses in Fig. 1 with a uniform magnetic field of approximately 600 G.

In the course of this work two types of collision chambers have been employed. Descriptions of these follow.

### Conventional Collision Chamber

This is shown schematically in Fig. 1. It is a conventional design consisting of a box in which the ions are formed and are allowed to escape through a large-area aperture, covered with mesh to reduce field penetration into the collision chamber from subsequent electrodes. On the wall of the collision chamber opposite the ion exit aperture is mounted a repeller plate. The application of a few volts to this electrode, of polarity such as to repel the ions towards the ion exit aperture, has only a small effect on the collection efficiency of fragment ions produced with initial kinetic energies of the order of 1 eV. In experiments of this type where one is

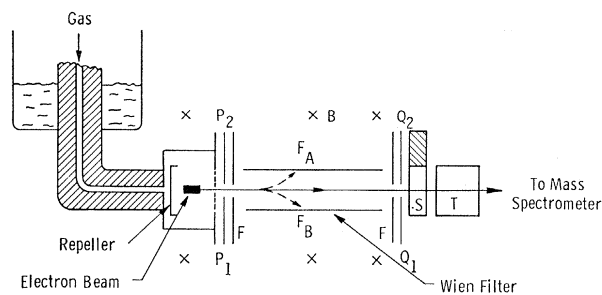


FIG. 1. Diagram of the electrode system, showing the "conventional" collision chamber and the ion velocity (Wien) filter.

<sup>7</sup> R. E. Fox, W. M. Hickam, D. J. Grove, and J. Kjeldaa, *Rev. Sci. Instr.* **26**, 1101 (1955).

attempting to control within rather close limits ( $\sim \pm 0.1$  eV) the energy of electrons within the collision chamber, the use of a large ion extraction field is to be avoided because it causes variations in potential along the electron beam. In the present case the potential of the repeller was in general made only sufficiently negative to ensure that, when taking electron retarding curves for calibration of the electron energy scale, the electron beam was retarded in space within the collision chamber.<sup>8</sup>

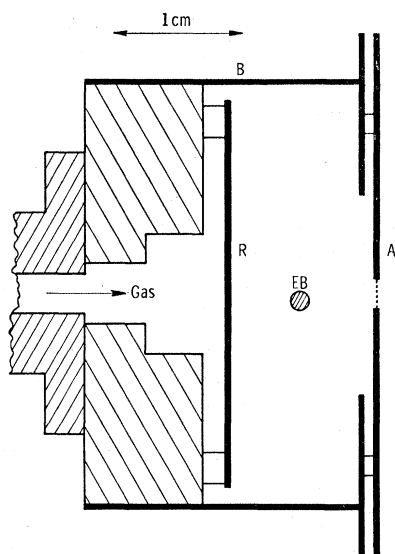
### "Split" Collision Chamber

The second design of collision chamber used is shown in Fig. 2. It consists of three electrically separate parts.<sup>9</sup> On one wall of the collision chamber box *B* is mounted a large-area plane repeller electrode *R*. The opposite wall of the chamber consists of an "attractor" electrode *A* containing a rather large, mesh covered slit. The whole assembly forms a reasonably gas-tight box, the attractor being separated from the collision chamber box by a circular glass gasket ground flat to provide good mating surfaces. This design offers many advantages over the conventional source. In particular, by holding the collision chamber box at a suitable potential between that of the repeller and the attractor, the extraction field produced between the attractor and repeller does not give rise to potential variations along the electron beam. Thus one is able to use extraction fields considerably larger than in a conventional source without degrading the electron energy resolution. It has been demonstrated that, with suitably chosen potentials applied to *A*, *B*, and *R*, the spread in energy produced by using large extraction fields arises primarily from the variation in potential transverse to the electron beam. That is, a spread in the electron energy is induced equal to the electron beam width multiplied by the extraction field strength. In the measurements reported here extraction fields of 0.4 V/cm or less are employed, and since the diameter of the electron beam is approximately 0.05 cm, an induced electron energy spread of no more than 20 mV is expected. The remaining parts of the ap-

<sup>8</sup> To ensure that the electron beam is retarded *in the volume* of the collision chamber a small negative potential is applied to the repeller, with respect to the rest of the collision chamber. The choice of this potential is made in the following way. Retarding curves are taken for various values of the repeller voltage measured with respect to the collision chamber. It is found that for repeller voltages  $V_R$  more negative than a certain value  $V_R(0)$  the position of the retarding curve is strongly dependent on  $V_R$ . For  $V_R > V_R(0)$  the position of the retarding curve is only weakly dependent on  $V_R$ . These two distinct regions correspond, respectively, to the electron beam being retarded by the negative space potential within the volume of the collision chamber imposed by the repeller potential, and to being retarded at the entrance or exit slit of the collision chamber, whichever happens to be the more negative. It is obvious that only in the former situation may the retarding curve be used to determine the energy the electrons have within the collision chamber. For actual operation of the ion source,  $V_R$  is made a few tenths of a volt negative to  $V_R(0)$ .

<sup>9</sup> This type of design has been used in the past by P. L. Randolph and R. Geballe (see Ref. 13), and possibly by others.

FIG. 2. Section through the "split" collision chamber. *A* is the attractor electrode; *R* the repeller. The electron beam *EB* enters and leaves the collision chamber box *B* through small orifices.



paratus, described below, were the same for both collision chambers.

#### The Wien Filter

On leaving the collision chamber the ions are velocity analyzed in a "Wien filter," i.e., a crossed magnetic and electric field velocity analyzer, consisting of electrodes *F*, *F<sub>A</sub>*, and *F<sub>B</sub>*. Before entering the Wien filter, the ions pass a split plate (*P<sub>1</sub>*, *P<sub>2</sub>*) forming a slit of 0.1 cm width. Between the two halves of electrode *P* a difference voltage of usually less than 2 V is applied to correct for the effects of the magnetic field on the ion trajectory prior to entering the filter, allowing the current entering the filter proper *F* to be maximized. The Wien filter, of length 2.5 cm, has entrance and exit slits 0.05 cm width, 1.4 cm long. The condenser plates *F<sub>A</sub>* and *F<sub>B</sub>* are placed symmetrically with respect to the axis of the tube and the potential applied between them provides a cross field *E*, such that ions of velocity  $v = E/B$  pass through the filter.<sup>10</sup> Electrode *Q*, which is split, performs a similar function to electrode *P*, serving to keep the ions on an approximately straight course, in the plane of the diagram, into electrode *S* which is a simple baffle designed to intercept those ions which have traversed the filter at large angles ( $> 8^\circ$ ) to the axis in the plane perpendicular to the diagram. Such ions would appear as a signal at the wrong energy, since the filter is only sensitive to the ion velocity along the axis. The face of this baffle adjacent to the following cylindrical electrode (*T*) is covered with mesh to reduce field penetration from the large voltage ( $\sim 100$  V) applied to electrode *T*, where the ions are accelerated to an energy at which they are no longer seriously influenced by the magnetic field of the Wien filter. The

<sup>10</sup> The equations of motion of a charged particle in crossed electric and magnetic fields are available in many textbooks. See, for example, J. R. Pierce, *Theory and Design of Electron Beams* (D. Van Nostrand, Inc., New York, 1949), Chap. 3.

electrode system shown in Fig. 1 is surrounded by an open-ended metal cylinder which extends as far as electrode *T* and is held at the potential of the collision chamber, i.e., ground. This cylinder serves to shield the electrode system from the metal vacuum envelope, which is held at the potential required to accelerate the ions to the energy at which they are mass-analyzed, usually +500V. On leaving electrode *T* the ions "see" the vacuum envelope potential and are consequently accelerated to the required energy.

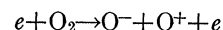
#### The Mass Spectrometer

The mass spectrometer is a  $90^\circ$  sector magnet instrument. The resolution is purposely kept low ( $\sim 30$ ) in these experiments in order to avoid the necessity of simultaneously tuning the mass-spectrometer and the Wien filter when scanning ion energies. On leaving the mass spectrometer, ions strike the first dynode of a ten-stage secondary electron multiplier, the output of which is detected by a vibrating-reed electrometer operated at 1000–2000 V positive with respect to ground potential. A servo-amplifier<sup>11</sup> is used to bring the output of the electrometer back to ground potential.

#### Measurement of Ion Energy

The instrument is used to scan the ion energies in the following way. The series of electrodes *P*, *F*, *F<sub>A</sub>*, *F<sub>B</sub>*, *Q*, and *S* are tuned to transmit selectively ions of a certain energy, usually about 2 eV. The voltage between electrodes *F* and the collision chamber is then swept over the appropriate range, and the ion current plotted, either manually or automatically, as a function of this voltage. Thus, ions formed with greater kinetic energy will appear at correspondingly lower accelerating voltages. While sweeping this voltage the potentials of the electron gun, and of the repeller remain constant relative to the collision chamber, and similarly the potentials of electrodes *P*, *Q*, and *S* remain constant relative to the potential of *F*.

In the measurements reported here the ion energy scale was obtained from the ion accelerating voltage scale by observing  $O^-$  ions produced by the pair-production process



which has an appearance potential of 17.2 eV. The sharp onset of this process, observed also in previous work,<sup>12</sup> and the observation in the present work that the peak in the ion energy distribution is relatively sharp and insensitive to electron energy within a few volts of threshold are strong indications that the  $O^+ + O^-$  potential-energy curve involved rises above the dis-

<sup>11</sup> G. J. Schulz, *Phys. Rev.* **135**, A998 (1964).

<sup>12</sup> The pair-production process has been observed by a number of workers. See, for example, J. D. Craggs, R. Thorburn, and B. A. Tozer, *Proc. Roy. Soc. (London)* **A240**, 473 (1957). The most detailed study is probably that of P. L. Randolph and R. Geballe, available as University of Washington Technical Report No. 6, 1958 (unpublished).

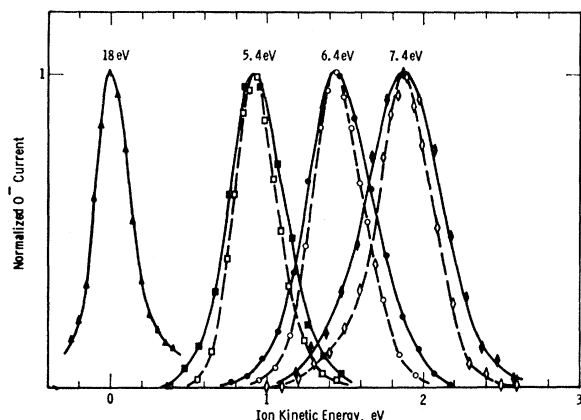


FIG. 3. Kinetic-energy distributions observed at the electron energies indicated. Data represented by filled points and full curves were taken with room-temperature gas; the open points and broken curves represent data taken with the gas inlet cooled with liquid nitrogen. The energy distribution resulting from pair production, using 18-eV electrons, is used to calibrate the ion energy scale.

sociation limit at an internuclear separation close to or less than the equilibrium separation of the ground state of  $O_2$ . Only in such a situation<sup>13</sup> does one expect the observed behavior of the cross section and ion energy distribution as a function of energy. In this situation the peak in the ion energy distribution must be at or very close to zero energy.<sup>14</sup> As shown in Fig. 3 we therefore use the position of the pair-production  $O^-$  peak, taken near threshold, to determine the zero of the ion energy scale.

The instrumental ion energy resolution obtained in the present studies is believed to be such that the instrumental half-width  $W_{1/2}(I)$  is approximately 0.2 eV. Such a figure is consistent with the observed width of zero kinetic energy  $O^-$  produced by pair production, shown in Fig. 3, and with the temperature dependence studies, discussed later. Also, in studying parent ions, for example  $O_2^+$ , which are formed with zero kinetic energy, the measured half-width  $W_{1/2}(M)$  is equal to  $W_{1/2}(I)$ , and has been shown to be related to the energy at which the ions are transmitted through the filter  $E_F$  by the empirical relation  $E_F/W_{1/2}(I) \approx 10$ . For  $E_F < 1$  eV this relation no longer holds,  $W_{1/2}(I)$  tending to a minimum realizable value of about 0.055 eV for  $E_F \leq 0.4$  eV. In the present case we use  $E_F \approx 2.0$  eV, and thus we expect  $W_{1/2}(I) \approx 0.2$  eV.

#### Calibration of the Electron Energy Scale

When using the conventional collision chamber, the electron energy scale was calibrated by taking retarding

<sup>13</sup> See Fig. 1 and accompanying discussion of H. D. Hagstrum, *Rev. Mod. Phys.* **23**, 185 (1951).

<sup>14</sup> This has been verified by showing that, in a mixture of  $O_2$  and CO,  $O^-$  produced by the pair-production process in  $O_2$  appears at the same ion accelerating voltage as  $O^-$  produced at the threshold of dissociative attachment in CO, which is such that the ions must have zero energy.

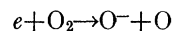
curves of the transmitted electron current as a function of electron accelerating voltage. In so doing the electron collector is maintained at a sufficiently high positive potential, usually a few volts, with respect to the collision chamber, so that the collected current is saturated; that is, insensitive to changes in the collector potential. The repeller potential was always such that the electrons were retarded in the volume of the collision chamber.<sup>8</sup>

The electron energy scale so determined is such that, in the difference distribution,<sup>15</sup> as many electrons have energies greater than this value as have energies less than this. This quantity may be determined by inspection of the difference retarding curve, being given by the difference between the accelerating voltage used and the voltage at which the difference current is retarded to one-half of its usual value.

When using the "split" source, advantage was taken of the feature that "total" ion current measurements may be made on either the repeller or the attractor. Thus, with the same potentials applied within the source, one may study the mass-analyzed  $O^-$  sample escaping through the slit in the attractor, the "total"  $O^-$  current arriving at the attractor, and the current of positive ions arriving at the repeller. In the present work this facility allowed the electron energy scale to be calibrated at three separate points: From the position of the "total"  $O^-$  dissociative attachment peak, the threshold for  $O^-$  produced by pair production, and from the threshold for positive-ion production. The same correction to the electron accelerating voltage scale placed these three points at  $6.7 \pm 0.1$  eV,  $17.2 \pm 0.1$  eV, and  $12.2 \pm 0.1$  eV, respectively, on the electron energy scale.<sup>16</sup>

### III. RESULTS

The dependence of the width of the energy distribution of  $O^-$  produced from  $O_2$  by the reaction



<sup>15</sup> In general, a difference voltage of 0.1 or 0.15 V was used, giving a difference electron distribution containing approximately 65% of the electrons in a 0.1-V slice. Since in the present measurements we are particularly interested in relating the most probable ion energy to the electron energy, it would be preferable to have the electron energy scale referred to the most probable electron energy of the difference distribution. If the difference distribution is approximately symmetrical, as it is found to be, such a scale would differ from that used here by only a few hundredths of a volt.

<sup>16</sup> The appearance potentials quoted were obtained by linear extrapolation of the ion current to the zero signal level, and therefore apply to the peak of the electron energy distribution. No attempt was made to resolve vibrational structure in the  $O_2^+$  appearance potential data. Thus the value of 12.2 eV quoted may well exceed the true ionization potential of  $O_2$ . [See J. W. McGowan, E. M. Clarke, H. P. Hanson, and R. F. Stebbings, *Phys. Rev. Letters* **13**, 620 (1964); J. A. R. Samson and R. B. Cairns, *J. Opt. Soc. Am.* **56**, 769 (1966)]. It does, however, agree with previous similar determinations [see for example C. E. Brion, *J. Chem. Phys.* **40**, 2995 (1964)], and as such is a check on the energy scale calibration.

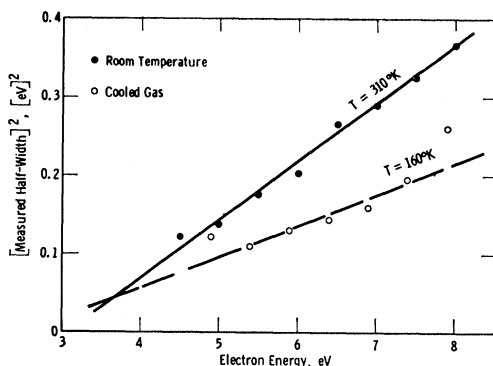


FIG. 4. A plot of the square of the measured half-width of the  $O^-$  ion kinetic-energy distribution versus the electron energy used. The temperatures indicated are obtained from the slopes of the straight lines drawn through the sets of experimental points.

on the electron energy and the gas temperature has been studied. Measurements have been made, at room temperature, of the position of the peak of the ion energy distribution, as a function of electron energy, from which a value for the electron affinity of atomic oxygen is deduced.

#### Ion Energy Distributions

Typical measured ion energy distributions are shown in Fig. 3. The points, through which the curves have been drawn, are experimental determinations of the difference ion current, normalized to give equal peak heights to facilitate visual comparison of the peak widths. The full curves, drawn through the solid points, refer to data taken with the gas at room temperature.<sup>17</sup> The dashed curves, and open points, refer to data taken with the gas inlet line cooled with liquid nitrogen. The electron energy used is indicated on each curve.

The single peak to the left represents  $O^-$  formed by pair production, and is used to calibrate the ion energy scale, as discussed in Sec. II. It is clear from Fig. 3 that the width of the ion energy distribution increases with increasing electron energy, and at a given electron energy, decreases with decreasing temperature. According to Eq. (6), a plot of the square of the half-width as a function of electron energy should lie on a straight line whose slope is determined by the gas temperature. Such a plot is shown in Fig. 4, where the solid points correspond to data taken at room temperature and the open points are obtained with the gas-inlet line cooled with liquid nitrogen. The measured half-widths must be expected to exceed the theoretically predicted widths because of instrumental broadening arising from the finite spread in electron energy and the finite resolution of the energy analyzer. Assuming that the real width

<sup>17</sup> Use of the term "at room temperature" here and elsewhere in the paper implies that no attempt was made to control the temperature of the gas inlet line, or of the collision chamber. Under these conditions, the temperature of the collision chamber is likely to be somewhat above that of the room, because of the proximity, within the vacuum system, of the electron-gun filament.

$W_{1/2}$  and the instrumental width  $W_{1/2}(I)$  add as the sum of their squares,<sup>18</sup> the measured half-widths  $W_{1/2}(M)$  will be given by

$$W_{1/2}^2(M) = W_{1/2}^2 + W_{1/2}^2(I),$$

where  $W_{1/2}^2$  is given by Eq. (6). Data taken at different gas temperatures are expected to lie on two straight lines whose point of intersection is given by  $(D-A)$  on the electron energy scale and by the square of the instrumental width on the  $W_{1/2}^2(M)$  scale. The data of Fig. 4 are seen to be consistent with such an interpretation. The straight lines drawn through the two sets of data correspond to gas temperatures<sup>19</sup> of 310 and 160°K. Their point of intersection while being rather ill-defined because of scatter in the data points, is consistent with the value of  $(D-A) = 3.6$  determined by a more accurate method described in the next subsection and with the expected instrumental half-width of approximately 0.2 eV. In fitting a straight line to the low-temperature data, less weight has been given to the first and last open points, which consistently lay above the trend of the remaining data. It is believed that this effect is instrumental, possibly arising from the fact that at these energies the finite spread in electron energies is being folded into a cross section which is a strong function of electron energy.

The points shown in Fig. 4 represent a single set of data for each temperature, taken with use of the R. P. D. technique. Numerous other data points obtained without use of the R. P. D. technique confirm the behavior shown, the straight-line fits being higher by approximately 0.02 on the  $W_{1/2}^2(M)$  scale because of the increased value of the instrumental width  $W_{1/2}(I)$ .

#### Determination of the Electron Affinity of O

As was pointed out in Sec. I, the position of the peak of the ion energy distribution (the most probable ion energy) serves to determine  $E_0$ , the quantity defined by Eq. (3). The results of such measurements are shown in Fig. 5, in which the most probable ion energy is plotted as a function of electron energy. Two sets of data are shown. The straight line, of slope  $1 - \beta = \frac{1}{2}$ , was chosen visually as the best fit to the data and serves to determine the intercept on the  $V_e$  axis. According to Eq. (3), this value of  $V_e$  determines  $(D-A)$ , the difference between the dissociation energy of  $O_2$  and the electron affinity of O. Knowing the value of  $D$  (5.11

<sup>18</sup> This would be the case if both were Gaussian. In the present situation this is not so, but deviations from the assumed addition rule are not expected to be serious.

<sup>19</sup> A separate determination of the gas temperature in the collision chamber has not been made. With the gas inlet tube cooled to 77°K with liquid nitrogen, the gas in the chamber is apparently at a temperature significantly above this, suggesting that either the gas does not reach equilibrium with the walls of the gas inlet tube, or that the thin walls (0.6 mm Advance) of the actual collision chamber, being exposed to the heating effect of the filament, do not reach the temperature of the heavy copper gas inlet tube.

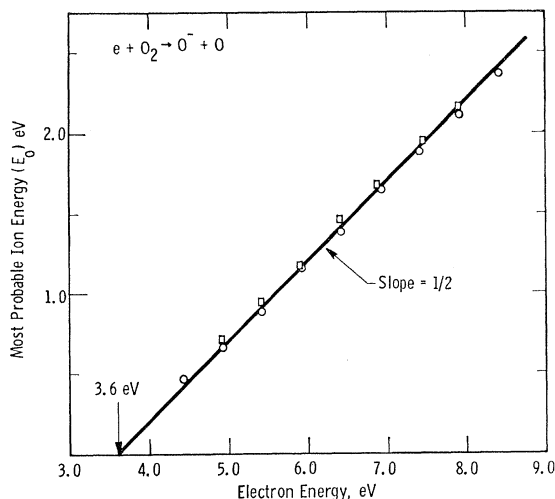


FIG. 5. A plot of the most probable ion energy versus the electron energy used. The straight line, of slope  $\frac{1}{2}$  prescribed by Eq. (3), is drawn through the two sets of experimental points shown, and intercepts the abscissa at  $(D-A)=3.6$  eV, from which we conclude that  $A=1.5$  eV.

eV),<sup>20</sup> we obtain a value for the electron affinity  $A$ , of atomic oxygen, of  $1.5 \pm 0.1$  eV. The precision with which  $(D-A)$  may be determined from Fig. 5 is somewhat better than the quoted probable error, which is believed to cover any inaccuracies in energy-scale calibrations.

In equating the position of the peak of the observed ion energy distribution to  $E_0$ , the most probable ion

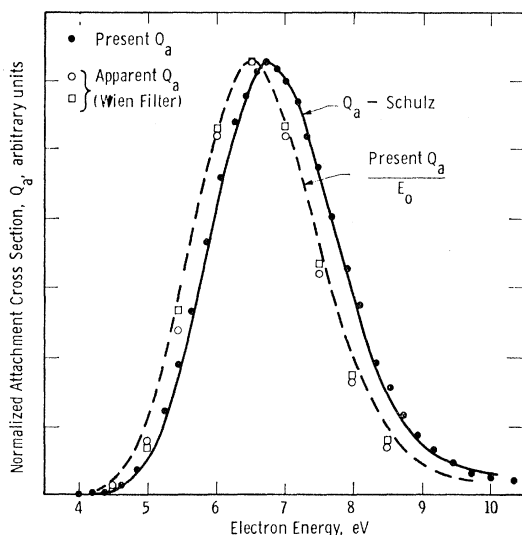


FIG. 6. This figure shows the effect of energy discrimination by the Wien filter system on the observed attachment cross section  $Q_a$ . The open points represent Wien filter data corrected for the widths of the ion energy distributions involved. The closed points are measurements of the "total" negative ion current to the attractor electrode (see Fig. 2). The full curve, shown for comparison, is the previously published data of Schulz (Ref. 2). The broken curve is obtained from the closed points by applying the weighting factor  $E_0^{-1}$ . All data are normalized to the same peak height.

<sup>20</sup> P. Brix and G. Herzberg, Can. J. Phys. 32, 110 (1954).

energy, it is important to establish that the peak shape is not seriously distorted by a variation of detection efficiency with initial ion energy. As a check that the detection efficiency did not depend strongly on initial ion kinetic energy over the range of interest here, measurements were made at various electron energies of the peak height and width, with constant gas pressure in the source, and with constant electron current. From Eq. (4) we note that, at the peak of the ion energy distribution the ion current will be proportional to  $E_0^{-1/2}$ . Thus the relative value of the attachment cross section at a given electron energy should be given by the product of the peak ion current and  $E_0^{1/2}$ . The Wien filter data corrected in this way is shown in Fig. 6 by the open squares. Alternatively, we note from Eq. (5) that  $E_0^{1/2}$  is proportional to the width,  $W_{1/2}$ , of the distribution and that we may therefore correct the data by multiplying the peak ion current by the width of the distribution. The Wien filter data corrected in this way is shown by the open-circle data points.

The closed-circle data points represent the electron energy dependence of the total negative-ion current collected by the attractor electrode of Fig. 2, which agree very closely with the previous measurements of Schulz<sup>2</sup>, shown by the full curve in Fig. 6.

The discrepancy in the shape of the cross section obtained from the Wien filter data may be assumed for the purposes of this discussion to be due entirely to energy discrimination effects associated with the Wien filter. If we assume that the detection efficiency varies as  $E^{-n}$ , the value<sup>21</sup> of the exponent  $n$  required to reconcile the shapes of the attachment cross-section peak measured by the above two methods is  $n=1.0 \pm 0.2$ . This is shown in Fig. 6 by the broken curve, which has been obtained from the present "total" data (the closed circles) by applying the weighting factor  $E_0^{-1}$ . All the data have been normalized to give the same peak height.

With the assumed analytic form of the energy discrimination, we may show that the peak of the observed ion energy distribution will be shifted an amount  $2n\beta kT$  from its true position. Thus we expect the position of the observed peak to be within 0.03 eV of its true value  $E_0$  for room-temperature gas.

#### IV. SUMMARY

A derivation of the distribution in ion energies expected from dissociative ionization or attachment processes shows that the thermal motion of the target gas causes a significant spread in the ion energies, which has in the past led to serious errors in the interpretation of retarding curves taken on the fragment ions. Direct measurements of the ion energy distributions resulting

<sup>21</sup> If the instrument accepts a small fixed range of velocities ( $-u$  to  $+u$ ) and ( $-w$  to  $+w$ ) in the directions transverse to the axis, and a variable axial velocity  $V$ , the acceptance solid angle will be  $\pi w w / V^2$ . Thus the empirically derived form of the energy discrimination ( $E^{-1}$ ) is seen to be reasonable.

from dissociative attachment of monoenergetic electrons to oxygen are consistent with the theoretical predictions. The electron affinity of atomic oxygen has been determined by a technique involving the direct measurement of the most probable ion energy as a function of electron energy, thus avoiding the difficulties associated with the interpretation of retarding curves. The electron affinity of atomic oxygen determined by the present measurements is  $A = 1.5 \pm 0.1$  eV, in excellent agreement with photodetachment threshold determinations.

### ACKNOWLEDGMENTS

The authors wish to acknowledge frequent discussions with the Atomic Physics Group at the Westinghouse Research Laboratories. We wish also to acknowledge the technical assistance of W. M. Uhlig, and of J. H. Kearney who also took much of the data reported in this paper.

### APPENDIX: DERIVATION OF ION ENERGY DISTRIBUTION

Let us consider ions of mass  $m$  having velocity  $V_0$  in the center-of-mass system, that is, relative to the center of mass of the target molecule of mass  $M$ , from which the ions are produced by reaction (1). The momentum of the impinging electron is neglected, being typically an order of magnitude less than the momentum of the target molecule at room temperature and for electron energies of the order of 10 V.

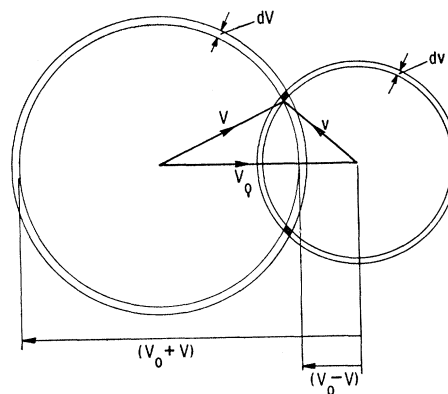
The velocity distribution of ions in the laboratory system is obtained by adding vectorially to  $V_0$  the initial velocity  $v$  of the target molecule in the laboratory system. The velocity space diagram is shown in Fig. 7, in terms of which we wish to calculate the fraction of ions whose velocity vectors terminate in the spherical shell of radius  $V$  and thickness  $dV$ .

Molecules having velocities before the impact in the range  $v$  to  $(v+dv)$  will contribute if their velocity vectors terminate within the intersection of the two spherical shells, shown shaded in the diagram. The fraction having velocity vectors terminating somewhere in the spherical shell of radius  $v$  and thickness  $dv$  is given by the usual Maxwellian distribution function. Of these, a fraction  $\rho$  terminates in the shaded ring. Since the distribution in  $v$  is isotropic,  $\rho$  is given by the ratio of the volume of the shaded ring to the volume of the whole shell of radius  $v$ , and one may show without difficulty that

$$\rho = VdV/2V_0v.$$

Thus, we require

$$\frac{dN}{N} = \int_{v=V_0-V}^{v=V_0+V} \frac{VdV}{2V_0v} 4\pi v^2 \left(\frac{M}{2\pi kT}\right)^{3/2} \exp\left[-\frac{M}{2kT}v^2\right] dv,$$



Velocity space diagram

Fig. 7. Velocity space diagram.  $V_0$  is the velocity of an ion relative to the center of mass of the parent molecule whose initial thermal velocity was  $v$ .  $V$  is the resulting ion velocity in the laboratory system.

the limits of integration being obvious from the diagram. Performing the integration we obtain

$$\frac{dN}{N} = \left(\frac{2M}{\pi kT}\right)^{1/2} \frac{V}{V_0} \exp\left[-\frac{M}{2kT}(V_0^2 + V^2)\right] \times \sinh\left(\frac{MV_0V}{kT}\right) dV. \quad (A1)$$

In the limit of  $V_0 \rightarrow 0$  this distribution reverts to a Maxwellian, corresponding to particles of mass  $M$  at temperature  $T$  as one would expect.

If  $MV_0V \gg kT$ , we may assume that

$$\exp[-MV_0V/kT] \ll 1,$$

and obtain

$$\frac{dN}{N} = \left(\frac{M}{2\pi kT}\right)^{1/2} \frac{V}{V_0} \exp\left[-\frac{M}{2kT}(V - V_0)^2\right] dV. \quad (A2)$$

In terms of  $E (= \frac{1}{2}mV^2)$  and  $E_0 (= \frac{1}{2}mV_0^2)$  we obtain the energy distribution

$$\frac{dN}{N} = \left(\frac{1}{4\pi\beta kTE_0}\right)^{1/2} \exp\left[-\frac{(E^{1/2} - E_0^{1/2})^2}{\beta kT}\right] dE \quad (A3)$$

given in the text and in Ref. 4.

The error involved in this expression will be less than 1% provided  $\exp(-2MV_0V/kT) < 0.01$ . In terms of the energies, this restriction becomes

$$(E_0E)^{1/2} > 1.16\beta kT. \quad (A4)$$

Since  $E$  is of the order of  $E_0$ , and  $\beta < 1$ , we expect inequality (A4) to be satisfied provided  $E_0 \gg kT$ , which is the criterion adopted in the text.